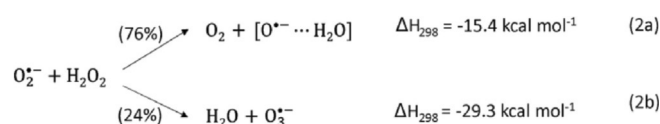


Spin-Forbidden Branching in the Mechanism of the Intrinsic Haber–Weiss Reaction

Ezequiel F. V. Leitão,^[a] Elizete Ventura,^[a] Miguel A. F. de Souza,^[c] José M. Riveros,^{*,[b]} and Silmar A. do Monte^{*,[a]}

The mechanism of the $O_2^{\cdot-}$ and H_2O_2 reaction (Haber–Weiss) under solvent-free conditions has been characterized at the DFT and CCSD(T) level of theory to account for the ease of this reaction in the gas phase and the formation of two different set of products (Blanksby et al., *Angew. Chem. Int. Ed.* **2007**, *46*, 4948). The reaction is shown to proceed through an electron-transfer process from the superoxide anion to hydrogen peroxide, along two pathways. While the $O_3^{\cdot-} + H_2O$ products are formed from a spin-allowed reaction (on the doublet surface), the preferred products, $O^-(H_2O) + {}^3O_2$, are formed through a spin-forbidden reaction as a result of a favorable crossing point between the doublet and quartet surface. Plausible reasons for the preference toward the latter set are given in terms of the characteristics of the minimum energy crossing point (MECP) and the stability of an intermediate formed (after the MECP) in the quartet surface. These unique results show that these two pathways are associated with a bifurcation, yielding spin-dependent products.

comes very slow^[3] or negligible^[4] in aqueous solutions under physiological conditions. Surprisingly, it has recently been observed to be very facile in the gas-phase under low-pressure conditions and to proceed directly in the absence of any solvent effects or catalyst.^[5] This finding suggests that the intrinsic HW reaction occurs with little or no activation energy and that it could occur easily in a hydrophobic environment. Two main features are particularly striking about the results obtained for the gas-phase reaction:^[5] 1) the rate constant amounts to 29% of the limiting-collision rate constant and 2) the nature and distribution of products, which are displayed in Scheme 1.



Scheme 1. Products identified by Blanksby et al.^[5] for the gas-phase reaction between superoxide and hydrogen peroxide.

The Haber–Weiss (HW) reaction:^[1]



has been the focus of much attention over the decades, because it can be a potential precursor of reactive oxygen species. Yet, the actual role of this reaction in biological processes and its suppression by the superoxide dismutase enzyme have been a matter of considerable controversy.^[2] Reaction (1) is known to proceed readily in the presence of Fe^{3+} ions (or other transition-metal ions) via a chain mechanism, but be-

Owing to the wide interest in the HW reaction and the unusual gas-phase results, the mechanism of this reaction poses some intriguing questions and provided the impetus for our investigation. Two possible mechanisms were originally envisioned for Reactions (2a) and (2b) in Scheme 1: initial formation of a stable ion-neutral complex $[O_2^{\cdot-} \cdots H_2O_2]$ followed by either a hydrogen atom or proton transfer, or by an electron transfer. In both cases, a series of putative intermediates were proposed to account for the final products. However, both mechanisms must overcome some *formal* unfavorable energetics. Proton transfer from H_2O_2 to $O_2^{\cdot-}$ is endothermic by 23 kcal mol⁻¹ in the gas phase,^[6] whereas an electron transfer from $O_2^{\cdot-}$ to H_2O_2 is also expected to be endothermic, because the electron affinity of H_2O_2 is presumably negative.^[7] In fact, experimental work as well as theoretical calculations for the $[H_2O_2]^{\cdot-}$ potential energy surface (PES) lead either to $O^-(H_2O)$ or $OH^-(OH)$ structures or to total dissociation.^[7,8] In addition, Reaction (2a) is exothermic, provided O_2 is formed in the ${}^3\Sigma_u^-$ ground state. This suggests that the major product of the intrinsic HW reaction proceeds through a spin-forbidden reaction pathway.^[9] By comparison, Reaction (1) in solution gives rise to singlet oxygen (${}^1\Delta_g^-$).^[10]

Herein, we report a detailed theoretical investigation of the relevant features of the PES for the $O_2^{\cdot-}/H_2O_2$ reaction to properly address the mechanism of the intrinsic HW reaction. Although the full computational details are described in the Supporting Information (Section S1), our discussion will be centered around the results obtained at the ROB2PLYP-D3/aug-cc-pVTZ//UB2PLYP-D3/aug-cc-pVTZ level of theory. This functional

[a] E. F. V. Leitão, Prof. E. Ventura, Prof. S. A. do Monte
Departamento de Química, Universidade Federal da Paraíba
João Pessoa, PB, 58.059–900 (Brazil)
E-mail: silmar@quimica.ufpb.br

[b] Prof. J. M. Riveros
Departamento de Química Fundamental, Universidade de São Paulo
Av. Prof. Lineu Prestes, 748, 05508-000, São Paulo, SP
Brazil João Pessoa, PB, 58.059–900 (Brazil)
E-mail: jmrnigra@iq.usp.br

[c] Prof. M. A. F. de Souza
Instituto de Química, Universidade Federal do Rio Grande do Norte
Natal, RN 59072-970 (Brazil)

Supporting Information for this article can be found under <http://dx.doi.org/10.1002/open.201600169>.

© 2017 The Authors. Published by Wiley-VCH Verlag GmbH & Co. KGaA. This is an open access article under the terms of the Creative Commons Attribution-NonCommercial License, which permits use, distribution and reproduction in any medium, provided the original work is properly cited and is not used for commercial purposes.

has been shown to yield comparable results with CCSD(T) for calculating reaction energies and transition states in a recent study of anion/neutral reactions.^[11] Dispersion corrections were included for cases involving large distances between fragments. Although the nature of this problem suggests a multi-configurational approach, attempts to describe these reactions at the CASSCF/MR-CISD level proved unsatisfactory, owing to difficulties in defining the same active space for all regions. However, the single reference approaches used here are shown to yield a correct description of the feasibility of these reactions and good agreement with experimental reaction enthalpies, as shown below. Similar single reference approaches have been applied successfully to other spin-forbidden reactions.^[19d]

Figures 1 and 2 illustrate the calculated energy profile and the optimized structures for the reactants (R), products (P), reactant complex (RC), product complexes (PC), intermediates (Int), transition states (TS), and the minimum-energy crossing point (MECP) between the doublet and quartet energy surfaces for the electron-transfer mechanism. The calculated reaction enthalpies at the ROB2PLYP-D3//UB2PLYP-D3/aug-cc-pVTZ level were estimated to be $-12.6 \text{ kcal mol}^{-1}$ for the ${}^2[\text{O}^-(\text{H}_2\text{O})] + {}^3\text{O}_2$ reaction and $-28.2 \text{ kcal mol}^{-1}$ for the ${}^2\text{O}_3^- + {}^1\text{H}_2\text{O}$ products, in good agreement with the experimental reaction enthalpies.^[5]

The reaction is predicted to proceed by the initial formation of a reactant complex, ${}^2\text{RC}$, between hydrogen peroxide and the superoxide anion (see Figures 1 and 2). This complex is calculated to be $31.7 \text{ kcal mol}^{-1}$ more stable than the reactants. This energy is considerably higher than the solvation energy of O_2^- with water that has been measured to range between 18.4 and $19.6 \text{ kcal mol}^{-1}$ from different experiments,^[12] and can be attributed to the larger number of hydrogen bonds in the ${}^2\text{RC}$ complex. The optimized structure for ${}^2\text{RC}$ reveals that the dihedral angle of H_2O_2 calculated to be approximately 113° for the isolated molecule is significantly decreased to almost 0.1° . Furthermore, the $\text{O}\cdots\text{H}$ distances are calculated to be 1.70 \AA , which are indicative of strong hydrogen bonds.^[13] From the

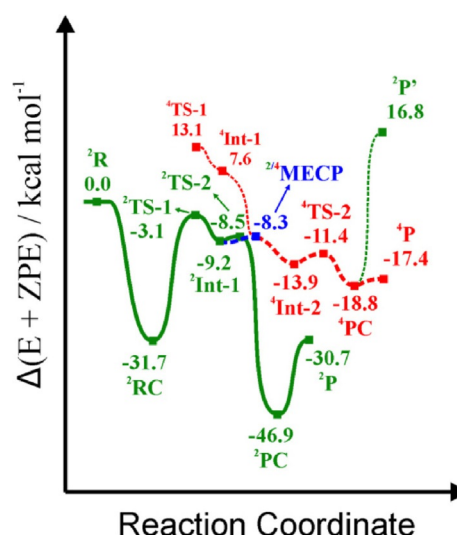


Figure 1. Calculated energy profile at the ROB2PLYP-D3//UB2PLYP-D3/aug-cc-pVTZ level for the electron-transfer mechanism of the $\text{O}_2^- + \text{H}_2\text{O}_2$ reaction. Relative energies of ${}^4\text{TS-1}$ and ${}^4\text{Int-1}$ (represented by the dashed thin line) do not include zero-point energies. ${}^2\text{P}'$ corresponds to the products with singlet dioxygen, ${}^2[\text{O}^-(\text{H}_2\text{O})] + {}^1\text{O}_2$. Refer to Figure 2 for the notation used.

${}^2\text{RC}$ complex, the electron-transfer pathway (Figure 1) proceeds through transition state ${}^2\text{TS-1}$ located $3.1 \text{ kcal mol}^{-1}$ below the energy of the reactants. The transition state ${}^2\text{TS-1}$ is characterized by partial charge transfer from the superoxide to the H_2O_2 moiety, as inferred from the approximately -0.4 NBO charge (calculated at the UB2PLYP-D3 level) on the superoxide anion. An analysis of the Kohn–Sham HOMO orbital (see Figure S4) with beta spin in the ${}^2\text{TS-1}$ doublet structure indicates a large contribution from the σ^* orbital of the O–O peroxide bond, and accounts for the increase in the bond distance. In the region between ${}^2\text{TS-1}$ and ${}^2\text{PC}$, the main rearrangements involve a combination of stretching of the hydrogen peroxide O–O bond, change in the relative orientation of the two OH groups, and migration of the O_2 moiety (see Figure 2), leading

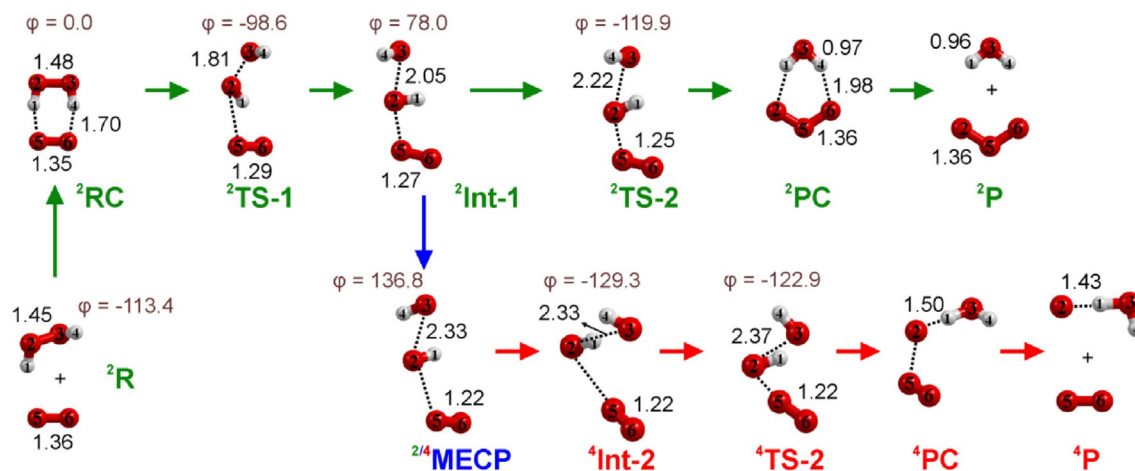


Figure 2. Calculated structures at the UB2PLYP-D3/aug-cc-pVTZ level for the electron-transfer mechanism of the $\text{O}_2^- + \text{H}_2\text{O}_2$ reaction. The main geometrical parameters (distances in \AA and $\varphi_{\text{H1-O2-O3-H4}}$ dihedral angles in degrees) are included in the structures.

to a higher entropy for ${}^2\text{TS-1}$ when compared with the tight ${}^2\text{RC}$ structure (see Table S1). From ${}^2\text{TS-1}$, this pathway leads to intermediate ${}^2\text{Int-1}$ calculated to be $9.2 \text{ kcal mol}^{-1}$ below the energy of the reactants, with a structure corresponding to a loose nonlinear $[\text{O}_2 \cdots \text{O}(\text{H}) \cdots \text{O}(\text{H})]^-$ complex. After ${}^2\text{Int-1}$, our results predict the system to evolve in the direction of products via a flat PES, with a topology that resembles a bifurcation containing a spin-forbidden pathway. On the one hand, formation of the ${}^2\text{O}_3^- + {}^1\text{H}_2\text{O}$ products (labeled as ${}^2\text{P}$) proceeds along the doublet surface through ${}^2\text{Int-1} \rightarrow {}^2\text{TS-2} \rightarrow {}^2\text{PC}$, which is characterized by a very low barrier (less than 1 kcal mol^{-1}). But, on the other hand, formation of ${}^2[\text{O}^-(\text{H}_2\text{O})] + {}^3\text{O}_2$ (labeled as the ${}^4\text{P}$ products) takes place via the ${}^2\text{Int-1} \rightarrow {}^{2/4}\text{MECP} \rightarrow {}^4\text{Int-2} \rightarrow {}^4\text{TS-2} \rightarrow {}^4\text{PC}$ route, consisting of a spin-forbidden pathway. The MECP structure connects two intermediates (${}^2\text{Int-1}$ and ${}^4\text{Int-2}$), one on each PES, with an energy difference of less than 1 kcal mol^{-1} between MECP and ${}^2\text{Int-1}$.

Single-point calculations were performed for the ${}^2\text{TS-1}$, ${}^2\text{Int-1}$, ${}^4\text{Int-2}$, and ${}^4\text{TS-2}$ structures to identify the spin-crossing region by changing the multiplicity from doublet to quartet and vice-versa (see the dashed thin line in Figure 1). Occurrence of a spin change, from ${}^2\text{Int-1}$ to ${}^4\text{Int-2}$, along with the quasi-degeneracy between the doublet and quartet states in the region between these two stationary points, suggests the presence of MECP (see Figures 1 and 2) between these two states after the ${}^2\text{TS-1}$ region. The NBO charges calculated for the MECP structure (taken as the average between the doublet and quartet charges) indicate complete charge transfer between the superoxide and the $[\text{OHOH}]$ moiety, with approximately equal charges on the two OH groups. Thus, the presence of O_2 leads to a charge separation with the negative charge in the H acceptor OH group, which is the reverse of what was predicted in the photodetachment experiments.^[8b]

From a structural point of view, the main difference between the two intermediates (${}^2\text{Int-1}$ and ${}^4\text{Int-2}$) is the relative position of the O_2 molecule. Although O_2 is almost in the same plane as the OH group closest to it in the doublet surface, O_2 is almost equidistant from the two OH groups in the quartet surface. Their NBO charges again indicate almost complete charge transfer between superoxide and the $[\text{OH} \cdots \text{OH}]$ moiety, with approximately equal charges in the two OH groups. These two intermediates then lead to their corresponding product complexes, namely $\text{O}_3^- \cdots (\text{H}_2\text{O})$ and $\text{O}_2 \cdots \text{O}^-(\text{H}_2\text{O})$, and finally to the O_3^- and $\text{O}^-(\text{H}_2\text{O})$ anions identified experimentally.^[5] In summary, our results indicate that O_3^- originates from the doublet surface, whereas the $\text{O}^-(\text{H}_2\text{O})$ anion is formed from the quartet surface (see Figures 1 and 2).

The larger O–O bond distances (see Figure 2) of O_2 in ${}^2\text{Int-1}$ and ${}^2\text{TS-2}$, when compared with those in ${}^4\text{Int-2}$ and ${}^4\text{TS-2}$, are consistent with singlet and triplet dioxygen in the doublet and quartet surfaces, respectively.^[14] This feature may account for the larger stability of the two points on the quartet surface (see Figure 1).

Accounting for the branching ratio that favors the preferential formation of $[\text{O}^-(\text{H}_2\text{O})] + {}^3\text{O}_2$ cannot be solely explained by the calculated energetics. This situation is similar to that described in Ref. [9b], where a stable species (in our case ${}^2\text{Int-1}$)

can either yield one set of products on the same PES (doublet) after passing through ${}^2\text{TS-2}$ (see Figure 1), or can form different products on another PES (quartet), with a spin change occurring at a crossing point (MECP in Figure 1). Although the ${}^4\text{Int-2}$ species is more stable than the ${}^2\text{Int-1}$, and may explain the preference for this pathway,^[9b] the energies of ${}^2\text{TS-2}$ and ${}^{2/4}\text{MECP}$ are essentially identical. In this case, the probability of the transition from the doublet to the quartet surface becomes important. Although a relatively small spin-orbit coupling matrix element can be expected for light elements, high probabilities of spin conversion can be achieved, depending on the characteristics of the two PES at the MECP^[15,16] and on the velocity of the system at the MECP.^[17] According to the transition probability based on the Landau–Zener model applied to spin-forbidden reactions, if, for instance, relatively low velocities (in comparison with the spin-orbit coupling between the two spin states) are achieved, the probability of spin conversion can be increased, as can be seen from Equation (1) of Ref. [17]. A preference for a spin-forbidden pathway has been observed previously for a reaction between species containing light elements,^[18] and many cases have been illustrated in gas-phase ion chemistry.^[19]

A potential energy calculation along the O...O bond distance of hydrogen peroxide and one of the O...OH bond angles shows a flat region involving ${}^2\text{Int-1}$, ${}^2\text{TS-2}$, and ${}^{2/4}\text{MECP}$ (see Figure 3). Recent studies of dynamics simulations suggest that the initial vibrational energy distribution and energy exchange between different degrees of freedom can determine the mechanisms and selectivity of reactions that occur on a PES with a flat topography.^[20] Figure 3 also displays two vibrational frequencies of the ${}^2\text{Int-1}$ related to the bending mode around the O...OH bending angle, which is consistent with the ${}^2\text{Int-1} \rightarrow {}^2\text{TS-2}$ route, and to the stretching mode responsible for separating the $\text{O}_2 \cdots \text{O}(\text{H}) \cdots \text{O}(\text{H})$ groups, associated with the ${}^2\text{Int-1} \rightarrow {}^{2/4}\text{MECP}$ pathway. Thus, preference for the spin-forbidden pathway for the $\text{O}_2 \cdot^- + \text{H}_2\text{O}_2$ reaction can be rationalized by the flatness of the doublet PES in combination with the fact

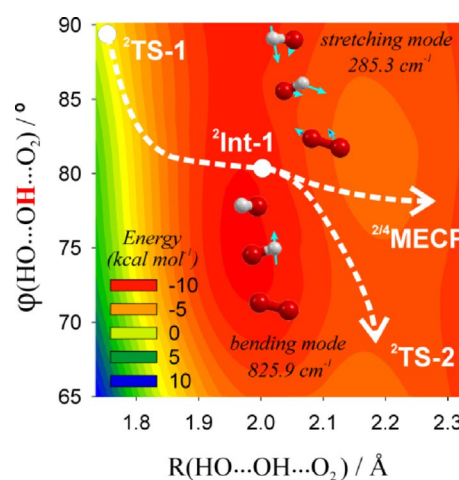


Figure 3. Contour map of the PES along the O...O bond distance of hydrogen peroxide and one of its O...OH bond angles, calculated by the relaxed-scan procedure at the ROB2PLYP-D3//UB2PLYP-D3/aug-cc-pVTZ level.

that the stretching mode (285.3 cm^{-1}) is energetically more readily accessible than the bending mode (825.9 cm^{-1}).

An alternative mechanism involving proton abstraction after the initial complex ${}^2\text{RC}$ has also been explored, which is fully described in the Supporting Information (see Section S3). Although the initial proton abstraction goes through a transition state below the energy of the reactants, the subsequent steps involve energies that are substantially higher than the energy of the reactants, either on the doublet or quartet surfaces. Thus, this mechanism is unlikely to be feasible under the experimental conditions of the gas-phase experiment,^[5] and cannot account for the ease of Reaction (2).

Our present study shows conclusively that the intrinsic HW reaction proceeds along a quartet and a doublet surface to yield $\text{O}^-(\text{H}_2\text{O}) + \text{O}_2$ and $\text{O}_3^- + \text{H}_2\text{O}$, respectively. The ease of these two pathways is associated with the larger stability of the stationary points and transition states compared to the isolated reactants and a very favorable crossing point between the two surfaces, with the experimentally observed preferred products corresponding to a spin-forbidden reaction. A particularly interesting observation is that the two pathways are derived from a bifurcation starting at the same transition state (${}^2\text{TTS-1}$, see Figure 3). To the best of our knowledge, it is the first time that a bifurcation yielding spin-dependent products is identified.

An initial comparison of the electron-transfer mechanism for the HW reaction in aqueous solution was also carried out using single-point calculations with the PCM continuum model.^[21] Although the calculated reaction free energy suggests that these channels are thermodynamically feasible, the obtained free energy of activation, corresponding to the first step, ${}^2\text{RC} \rightarrow {}^2\text{TTS-1}$, is very high, (ca. $31.3\text{ kcal mol}^{-1}$; see Table S1). This result agrees with the fact that the HW reaction is suppressed in aqueous solution.

Acknowledgements

Financial support from CAPES, CNPq, and FINEP (Brazilian agencies) has made this work possible.

Conflict of Interest

The authors declare no conflict of interest.

Keywords: density functional calculations • electron transfer • Haber–Weiss reaction • potential energy surfaces • spin-forbidden branching

- [1] F. Haber, J. Weiss, *Proc. R. Soc. London Ser. A* **1934**, *147*, 332.
- [2] a) J. P. Kehrer, *Toxicology* **2000**, *149*, 43; b) W. H. Koppenol, *Redox Rep.* **2001**, *6*, 229; c) S. L. Liochev, I. Fridovich, *Redox Rep.* **2001**, *7*, 55; d) C. Beauchamp, I. Fridovich, *J. Biol. Chem.* **1970**, *245*, 4641.
- [3] J. Weinstein, B. H. J. Bielski, *J. Am. Chem. Soc.* **1979**, *101*, 58.
- [4] B. Halliwell, *FEBS Lett.* **1976**, *72*, 8.
- [5] S. J. Blanksby, G. B. Ellison, V. M. Bierbaum, S. Kato, *Angew. Chem. Int. Ed.* **2007**, *46*, 4948; *Angew. Chem.* **2007**, *119*, 5036.
- [6] *NIST Chemistry WebBook*, NIST Standard Reference Database Number 69, Eds. P. J. Linstrom, W. G. Mallard.
- [7] J. Hrusák, H. Friedrichs, H. Schwarz, H. Razafinjanahary, H. Charmette, *J. Phys. Chem.* **1996**, *100*, 100.
- [8] a) D. Nandi, E. Krishnakumar, A. Rosa, W.-F. Schmidt, E. Illenberger, *Chem. Phys. Lett.* **2003**, *373*, 454; b) H.-J. Deyerl, T. G. Clements, A. K. Luong, R. E. Continetti, *J. Chem. Phys.* **2001**, *115*, 6931; c) B. M. Messer, D. E. Stielstra, C. D. Cappa, K. W. Scholtens, M. J. Elrods, *Int. J. Mass Spectrom.* **2000**, *197*, 219.
- [9] a) J. N. Harvey, *Phys. Chem. Chem. Phys.* **2007**, *9*, 331; b) J. N. Harvey, *WIREs Comput. Mol. Sci.* **2014**, *4*, 1.
- [10] a) A. U. Khan, M. Kasha, *Proc. Natl. Acad. Sci. USA* **1994**, *91*, 12365; b) For similar results with alkyl peroxides, see L. A. MacManus-Spencer, B. L. Edlund, K. McNeill, *J. Org. Chem.* **2006**, *71*, 796.
- [11] Y. G. Proenza, M. A. F. de Souza, E. Ventura, S. A. do Monte, R. L. Longo, *Phys. Chem. Chem. Phys.* **2014**, *16*, 26769.
- [12] a) M. Arshadi, P. Kebarle, *J. Phys. Chem.* **1970**, *74*, 1483; b) A. K. Luong, T. G. Clements, M. Sowa Resat, R. E. Continetti, *J. Chem. Phys.* **2001**, *114*, 3449.
- [13] G. A. Jeffrey, in *An Introduction to Hydrogen Bonding*, Oxford, University Press, New York, **1997**.
- [14] L. Bytautas, N. Matsunaga, K. Ruedenberg, *J. Chem. Phys.* **2010**, *132*, 074307.
- [15] A. O. Lykhin, D. S. Kaliakin, G. E. dePolo, A. A. Kuzubov, S. A. Varganov, *Int. J. Quantum Chem.* **2016**, *116*, 750.
- [16] S. Liu, S. Srinivasan, J. Tao, M. C. Grady, M. Soroush, A. M. Rappe, *J. Phys. Chem. A* **2014**, *118*, 9310.
- [17] S. Ahmadvand, R. R. Zaari, S. A. Varganov, *Astrophys. J.* **2014**, *795*, 173.
- [18] M. Besora, J. N. Harvey, *J. Chem. Phys.* **2008**, *129*, 044303.
- [19] a) J. N. Harvey, M. Aschi, H. Schwarz, W. Koch, *Theor. Chem. Acc.* **1998**, *99*, 95; b) M. Aschi, J. N. Harvey, C. Schalley, D. Schröder, H. Schwarz, *Chem. Commun.* **1998**, 531; c) D. Schröder, S. Shaik, H. Schwarz, *Acc. Chem. Res.* **2000**, *33*, 139; d) Z. Yang, B. Eichelberger, O. Martinez, Jr., M. Stepanovic, T. P. Snow, V. M. Bierbaum, *J. Am. Chem. Soc.* **2010**, *132*, 5812.
- [20] a) M. A. F. de Souza, E. Ventura, S. A. do Monte, J. M. Riveros, R. L. Longo, *Chem. Eur. J.* **2014**, *20*, 13742; b) Y. G. Proenza, M. A. F. de Souza, R. L. Longo, *Chem. Eur. J.* **2016**, *22*, 16220.
- [21] a) C. Adamo, V. Barone, *Chem. Phys.* **1999**, *110*, 6158; b) M. Cossi, N. Rega, G. Scalmani, V. Barone, *J. Comput. Chem.* **2003**, *24*, 669.

Received: December 20, 2016

Revised manuscript received: January 20, 2017

Version of record online March 23, 2017